




Düzce Üniversitesi Bilim ve Teknoloji Dergisi

Araştırma Makalesi

Comparative Study of Improvement of Hematite as Visible Light-Driven Photocatalyst by Doping with Zinc and Copper

 Emre Alp ^{a,*}

^a *Metallurgy and Materials Engineering Department, Bartın University, Bartın, Turkey*

** emrealp@bartin.edu.tr*

DOI: 10.29130/dubited.1051644

ABSTRACT

The low cost, earth abundance, nontoxic, and efficient photocatalysts materials have a critical role in order to solve environmental issues. In this regard, hematite (α -Fe₂O₃) has received significant attention due to its desirable properties. In the present study, zinc-doped and copper-doped hematite nanoparticles were synthesized by the hydrothermal method. The photocatalytic features of produced nanopowders were investigated. The evaluations of photocatalytic activities of synthesized nanoparticles were executed by monitoring the degradation rate of Rhodamine B (RhB) under the solar simulator in heterogeneous photocatalysis. Compared to commercial Degussa TiO₂ powder, the transition metal doped hematite (α -Fe₂O₃) samples showed better photocatalytic activities against RhB under the solar simulator. It was observed that even though there were no significant differences in their characteristic properties strongly affecting photocatalytic activity such as morphological features, optical absorption characteristics, and band gaps, Cu-doped α -Fe₂O₃ nanoparticles exhibited higher photocatalytic activity, which is %20 higher than the Zn-doped α -Fe₂O₃. The synthesized Cu-doped hematite nanoparticles are hopeful materials as a visible-light-driven photocatalytic material to degrade organic pollutants in aquatic media.

Keywords: *Hematite (α -Fe₂O₃), Zn-doped Hematite, Cu-doped Hematite, , Heterogeneous Photocatalysis*

Görünür-Işık ile Çalışan Fotokatalizör Hematitin Çinko ve Bakır ile Katkılanmasıyla Geliştirilmesinin Karşılaştırmalı İncelenmesi

Öz

Çevre ile ilgili konuların çözümünde, ucuz, bol bulunan, toksik olmayan ve verimli çalışan fotokatalitik malzemeler kritik role sahiptir. Bu açıdan, hematit (α -Fe₂O₃) istenen bu özelliklerden dolayı oldukça ilgi çekmektedir. Bu çalışmada, çinko katkılı ve bakır katkılı hematit nanopartiküller hidrotermal yöntem ile sentezlenmiştir. Üretilen nanotozların fotokatalitik özellikleri incelenmiştir. Sentezlenen nanopartiküllerin fotokatalitik aktivitesi güneş simülatörü altında Rodamin b.'yi parçalama performansı izlenerek belirlenmiştir. Geçiş metalleriyle katkılanmış hematit yapıların Rodamin b.'yi (RhB) parçalama verimi, ticari ürün Degussa TiO₂ tozlara göre daha yüksekti. Fotokatalitik aktiviteyi güçlü bir şekilde etkileyen ışık absorpsiyonu, morfolojik yapı ve optik bant genişliği gibi özellikler açısından büyük farklar olmasa da, Cu-katkılı α -Fe₂O₃ nanopartiküllerin, Zn-katkılı α -Fe₂O₃ nanopartiküllerden %20 kadar daha yüksek fotokatalitik aktive gösterdiği gözlemlendi. Sulu ortamlardaki organik kirliliklerin temizlenmesinde, Cu-katkılı α -Fe₂O₃ nanopartiküller görünür bölgede aktif fotokatalitik malzeme olarak umut verici bir malzemedir.

Anahtar Kelimeler: *Hematit (α -Fe₂O₃), Zn-katkılı hematit, Cu-katkılı hematit, Heterojen fotokataliz*

I. INTRODUCTION

High efficient photocatalytic nanomaterials are thought to have a crucial role to overcome some most important issues such as clean energy demands, environmental pollution, and global warming [1]. Recent studies have reported that hematite ($\alpha\text{-Fe}_2\text{O}_3$) is one of the most up-and-coming materials for solar-related applications due to its high physicochemical stability, low cost, nontoxicity, and narrow optical bandgap (1.9-2.2 eV) [2], which enables it to absorb more portion of solar irradiation relative to conventional photocatalytic materials, such as TiO_2 and ZnO . Although hematite has favorable properties to use in solar-related applications, it has some shortcomings. It suffers from poor electrical conductivity ($8 \times 10^{-6} - 2 \times 10^{-4} \Omega^{-1} \text{cm}^{-1}$) [3], short hole-diffusion length (2-4 nm) [3], low carrier mobility ($< 1 \text{ cm}^2 \text{V}^{-1} \text{s}^{-1}$) [4], low absorptivity (120 nm $\lambda=550$ nm) [5] and a very short excited-state lifetime (10^{-12} s) [6]. To overcome these shortcomings, there are various methods such as manipulation of morphological features [7, 8], surface treatments [9], plasmonic effects [10], and incorporation of dopants [11,12]. These mentioned inherent disadvantages of hematite semiconductors give rise to diminishing their photoactivity. To solve these limitations in the inherent of hematite and ameliorate its properties, doping is one of the effective methods. With this objective, several transition metals such as Sn [13], Ti [14], Mn [15], Zn [16], Mg [17], Nb [18], Cu [19], and Ta [20] have been doped into hematite ($\alpha\text{-Fe}_2\text{O}_3$) to improve the photocatalysis efficiency of hematite.

Up to now, various methods have been used to synthesize doped hematite nanostructures, including electrodeposition [21], co-precipitation technique [31], hydrothermal process [22]. Suman et al. [32] synthesized Zn-doped hematite nanopowders with varying concentrations by using a sol-gel process. They reported that the bandgap value of doped nanoparticles reduced relative to pure hematite and the lowest bandgap was Zn %4 doped hematite nanoparticles, belonging to those that were the highest photodegradation activity. Satheesh and co-workers [23] fabricated doped hematite nanoparticles with three different transition metals ($M = \text{Cu}, \text{Ni}, \text{and Co}$) by the co-precipitation method. They observed that Cu-doped hematite particles exhibited higher photocatalytic activity than Ni-doped and Co-doped hematite and moreover, it preserved its activity without significant loss after the four times photodegradation tests.

In the present study, the hydrothermal method was utilized to produce transition metal (Zinc-Zn and Copper-Cu) doped hematite nanoparticles. The photocatalytic efficiency of synthesized nano-particles was carried out by monitoring the degradation of RhB model dye under AM 1.5G solar simulator. The copper- and zinc-doped hematite nanoparticles did not show significant differences in terms of morphological features, optical absorption, and band gaps, but a remarkable difference in their photocatalytic performances was observed. It was observed that the doping with zinc and copper mightily affected the photocatalytic characteristic of nanopowders compared to the photocatalytic activity of commercial Degussa TiO_2 powder. The superior photocatalytic degradation efficiency was obtained with the copper doped hematite when compared to that of zinc doped hematite and the Degussa TiO_2 powder.

II. EXPERIMENTAL

A. CHEMICALS AND HYDROTHERMAL SYNTHESIS OF DOPED-HEMATITE NANOPARTICLES

Iron (III) nitrate nonahydrate ($\text{Fe}(\text{NO}_3)_3 \cdot 9\text{H}_2\text{O}$), zinc nitrate hexahydrate ($\text{Zn}(\text{NO}_3)_2 \cdot 6\text{H}_2\text{O}$), copper (II) nitrate hemi(pentahydrate) ($\text{Cu}(\text{NO}_3)_2 \cdot 2.5\text{H}_2\text{O}$), sodium carbonate (Na_2CO_3), urea (NH_2CONH_2), hydrogen peroxide 30% (H_2O_2), and rhodamine B ($\text{C}_{28}\text{H}_{31}\text{ClN}_2\text{O}_3$) were purchased from Sigma-Aldrich. All aqueous solutions were prepared with deionized (DI) water (18.2 M Ω /cm at 25 °C). All used chemicals were of analytical grade and used as received.

To produce the doped-hematite nanoparticles, 900 mg of iron nitrate nonahydrate, 1176 mg of sodium carbonate, and 75 mg urea were dissolved into 50 mL of DI water. These prepared solutions were the same for both nanoparticles fabricated with the different transition metals. Copper (II) nitrate hemi(pentahydrate) and zinc nitrate hexahydrate were added for producing Cu-doped hematite and Zn-doped hematite, respectively. The obtained solutions were transferred to a 100 ml Teflon-lined stainless-steel reactor and then, were placed into a furnace at 160 °C for 12 h. The as-synthesized particles were centrifuged and washed with ethanol and distilled water several times to provide the removal of residuals. Finally, the obtained products were dried overnight. Scheme 1 demonstrates the schematic drawings of the steps of the production procedures for fabricating doped hematite nanoparticles.

B. CHARACTERIZATION

The microstructural characteristics and chemical analyses of the synthesized doped-hematite nanoparticles were carried out via the field emission gun scanning electron microscope (FESEM). The phase characterization of synthesized nanoparticles was carried out by a RIGAKU SmartLab™ X-ray diffractometer with Cu-K α radiation ($\lambda = 1.5406 \text{ \AA}$) in the range 20-80°. The degradation rate of pollutants by synthesized nanoparticles during the photocatalytic test was monitored via UV-Vis-NIR spectrophotometers. Also, evaluation of optical band gap value and optical measurement related to doped-hematite nanoparticles were executed out by UV-Vis-NIR spectrophotometers.

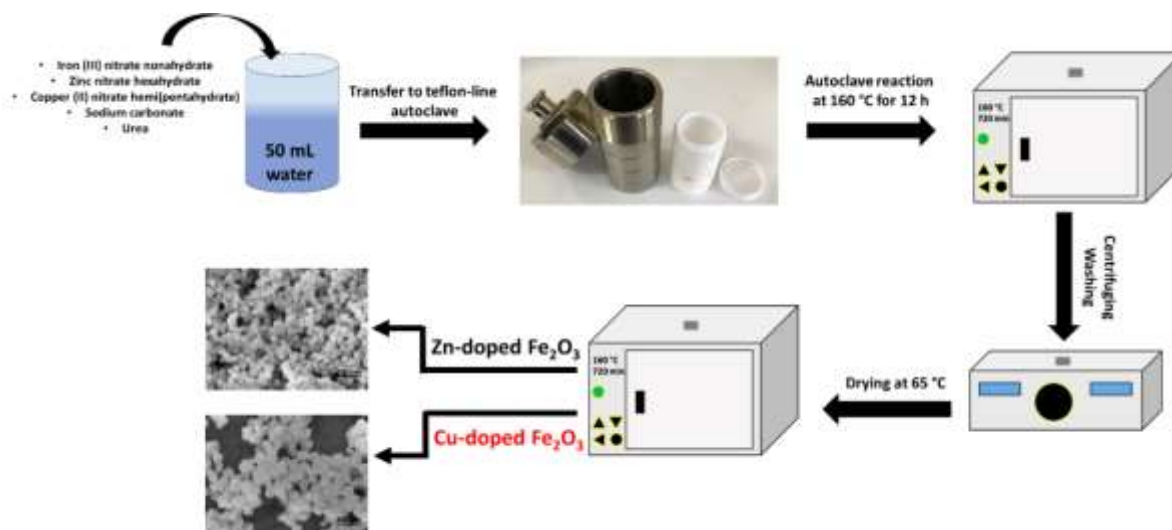


Figure 1. Schematic illustration of the production of transition metal-doped hematite.

C. PHOTOCATALYTIC PROPERTIES

The photocatalytic performances measurements of synthesized transition metal-doped hematite nanoparticles were executed against rhodamine B (RhB) dye in an atmospheric environment. The typically prepared solutions for evaluating the efficiency of produced nanoparticles had the identical concentration of pollutant model molecule (10 mg RhB /L) for all photocatalytic tests. Then, 40 mg of produced nanoparticle materials was added into solution (80 mL) involving the model pollutant, and the suspension was dispersed. 0,5 mL of hydrogen peroxide was added into suspensions as a sacrificial electron scavenger. Before photoexcitation, the suspensions were stirred in the dark for an adequate duration to provide adsorption stability. After the adsorption-desorption process, the suspensions homogeneously dispersed were put under a simulated solar light machine at 15 cm in distance away from the light spot with continuously magnetic stirring. By taking the sample from the suspension at a determined interval time, the photocatalytic degradation rates of the model pollutant were monitored via a spectrophotometer.

III. RESULTS AND DISCUSSION

The morphological characteristics, chemical analyses, and energy-dispersive X-ray spectroscopy (EDS) elemental maps of hydrothermally synthesized nanoparticles are presented in Figures 2-3. As seen from figure 2a-b, produced Zn-doped hematite powders were spherical morphology with an average of 50 nm in size. The fabricated nanoparticles were uniform size and shape distribution as seen from images represented in figure 1a-b. The energy-dispersive X-ray spectroscopy (EDS) analysis taken from Zn-doped hematite particles is given in Figure 2c-f, along with elemental mappings. The doping atomic zinc ratio to the hematite was determined as 1.2% by chemical analysis taken from a selected area in the sample.

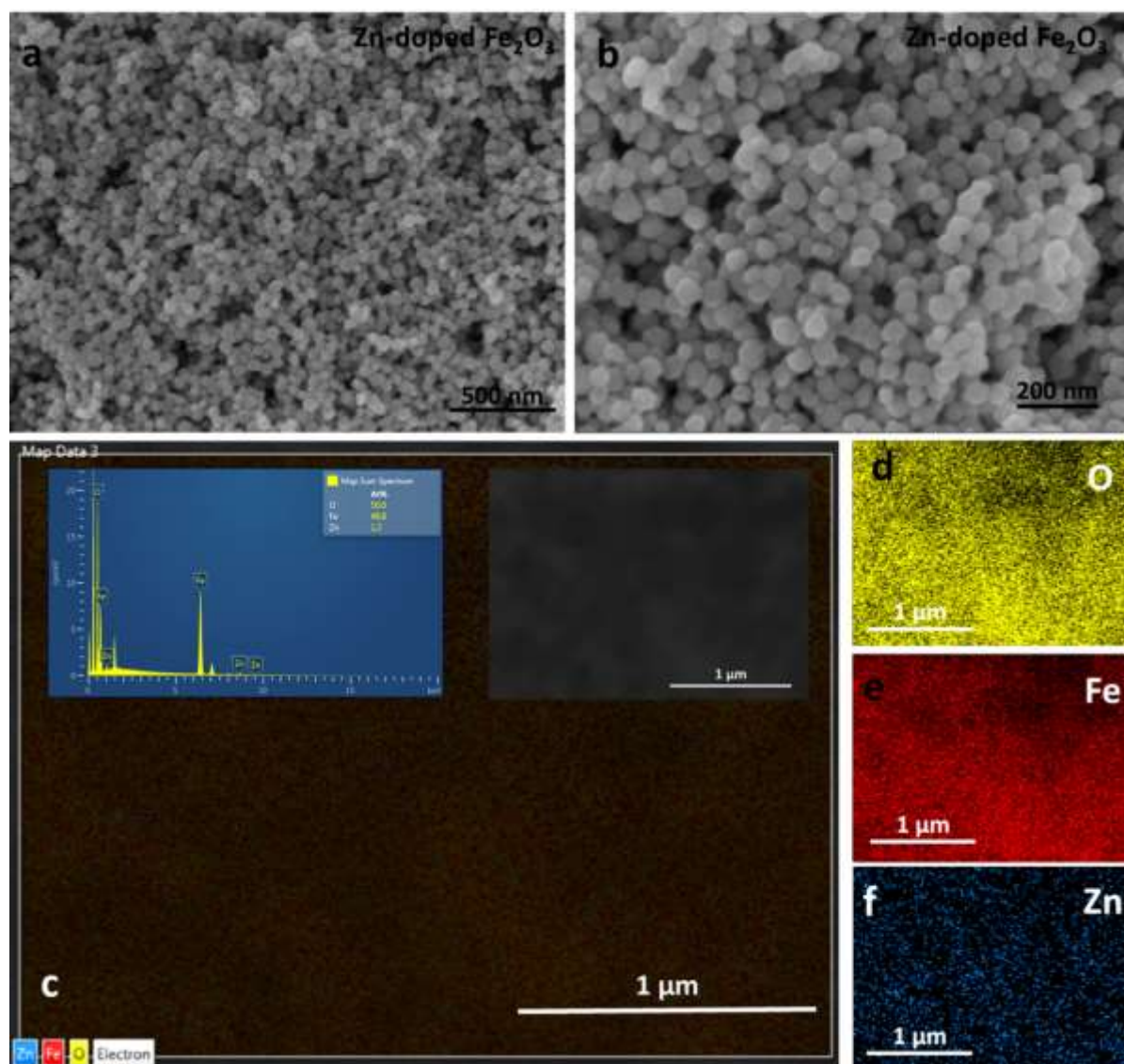


Figure 2. Representative Scanning Electron Microscopy images of the synthesized Zn-doped hematite (a-b). Chemical analysis and EDS elemental mapping of the synthesized Zn-doped hematite (c-f).

The electron microscopy images belonging to Cu-doped hematite nanoparticles are represented in figure 2a-b. Just like in Zn-doped hematite powders in terms of synthesizing homogeneity, their morphological features were also similar to Zn-doped hematite powders but too little larger than them. The doping copper ratio to the hematite was 2.9% at as seen in the EDS spectrum of synthesized particles given inset of figure 3c.

Phase analysis of the synthesized doped-hematite nanoparticles was executed via XRD and patterns belonging to related nanoparticles are presented in figure 3. All diffraction peaks of synthesized hematite nanoparticles are well-matched with JCPDS file data for Zn-doped hematite (drawn as a black line) and Cu-doped hematite (drawn as a red line), which are (012), (104), (110), (113), (024), (116), (214), and (300) peaks of the trigonal structure of the hematite phase (α -Fe₂O₃, space group: R-3c, lattice parameters of a = b = 0.503 nm and c = 1.373 nm, JCPDS file No. 33-0664). No other peak was observed except the hematite phase of iron oxide.

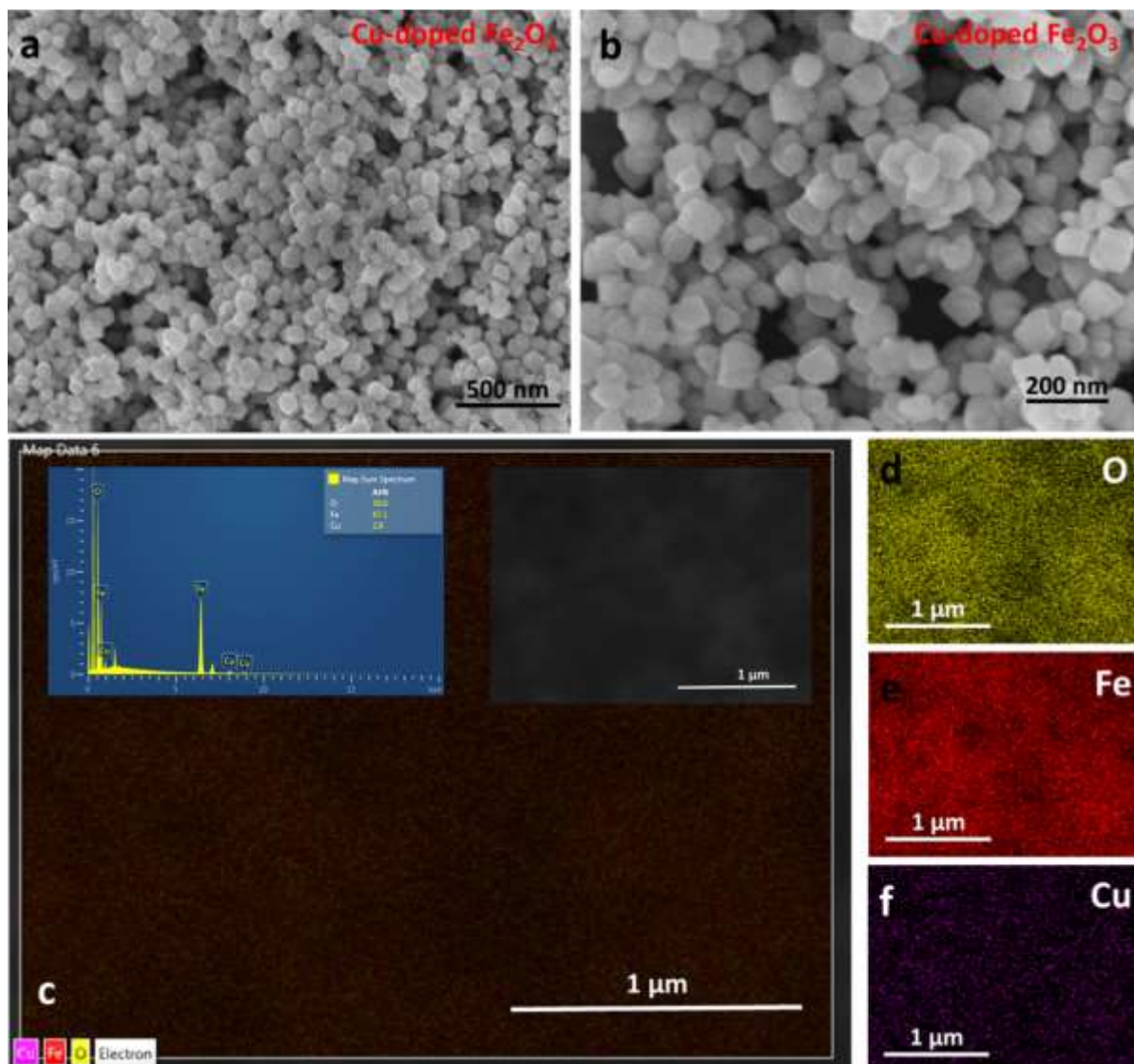


Figure 3. Representative Scanning Electron Microscopy images of the synthesized Cu-doped hematite (a-b). Chemical analysis and EDS elemental mapping of the synthesized Cu-doped hematite (c-f).

The absorption spectra and the estimated optical band gap values of the produced nanoparticles are given in figure 4. The absorption spectra represented in graphs were derived from using Kubelka-Munk (K-M) Theory [24]. Tauc's approximation given with the equation below is used to evaluate the optical band gap values of materials [25].

$$\alpha h\nu = A(h\nu - E_g)^n \quad (1)$$

In the equation, α is the extinction coefficient which is corresponding to $F(R)$ in the Kubelka-Munk theory. The other variables given in the equation are proportionality constant (A), optical band gap of

the semiconductor material (E_g : eV), light frequency (ν : s^{-1}), and Planck constant (h : J.s). The exponent n is a constant relating to the electronic transition type.

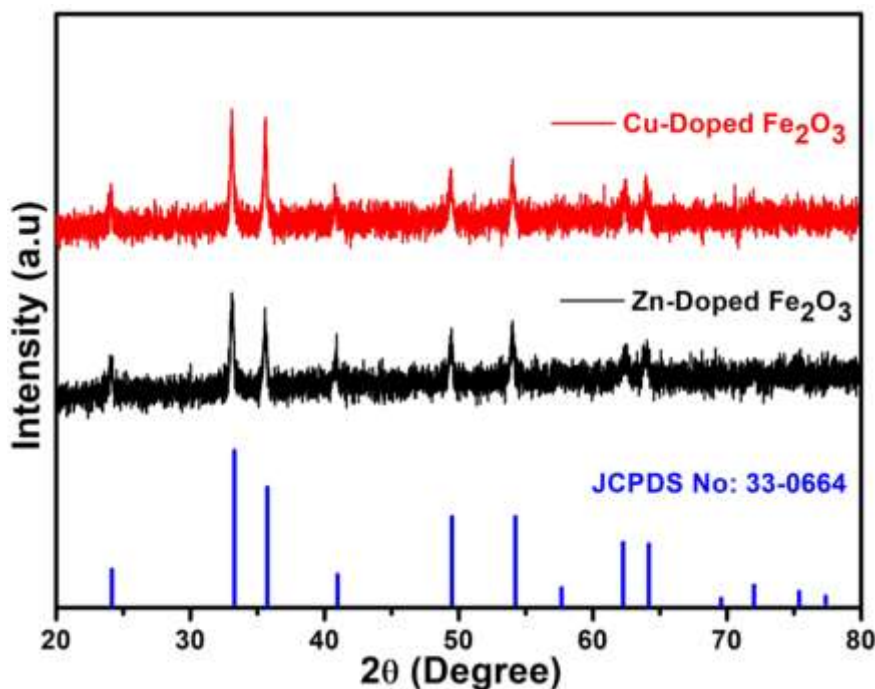


Figure 4. XRD diffraction pattern of synthesized doped-hematite particles. (Black pattern and red pattern designate Zn-doped hematite and Cu-doped hematite, respectively.)

In that study, the band type of hematite was taken into account as a direct allowed transition for determining its optical band gap value due to the fact that studies published in the literature [26,10] report that hematite had a direct allowed transition. For this reason, the optical bandgaps of produced powders were determined from the plot of $h\nu$ vs. $(F(R)h\nu)^2$ through extrapolating the straight portion to the energy axis at $\alpha=0$ in figure 4b and figure 4d. The optical bandgap of synthesized particles were calculated to be 2.01 eV and 2.03 eV for Cu-doped hematite and Zn-doped hematite, respectively. The determined optical band gap values for both synthesized nanoparticles were so close to each other. Similarly, it should be noted that the absorption vs. wavelength characteristics of powders were also quite identical. Even though these optical similarities, their photocatalytic performances were reasonably different from each other as would be seen in the following section.

It is known that in the heterogeneous photocatalytic processes, the elimination of pollutant effluents in aquatic media realizes by so-called reactive oxygen species (ROS), such as mainly hydroxyl radicals ($\cdot\text{OH}$), but also singlet oxygen ($^1\text{O}_2$) and superoxide anion radicals ($\cdot\text{O}_2^-$), etc [27]. In the presence of photocatalyst, the reactive oxygen species are produced by photogenerated holes (h^+) - electrons (e^-) pairs. The hydroxyl radicals ($\cdot\text{OH}$) as the reactive oxygen species, that are generated by photoinduced holes (h^+) - electrons (e^-) pairs, cause decoloration of dye molecule to harmless products in a photocatalysis process (as presented in a schematic demonstration in figure 5) [28, 29]. In this case study, photogenerated charge carriers in the hematite photocatalyst lead to produce hydroxyl radicals ($\cdot\text{OH}$) by trapping with hydrogen peroxide (H_2O_2), artificial electron scavenger. The behavior of electrons has two ways: they are caught by hydrogen peroxide to produce hydroxyl radicals and trapped by Fe^{+3} on the surface to create Fe^{+2} . The pathways of the degradation process could be given by reactions below:



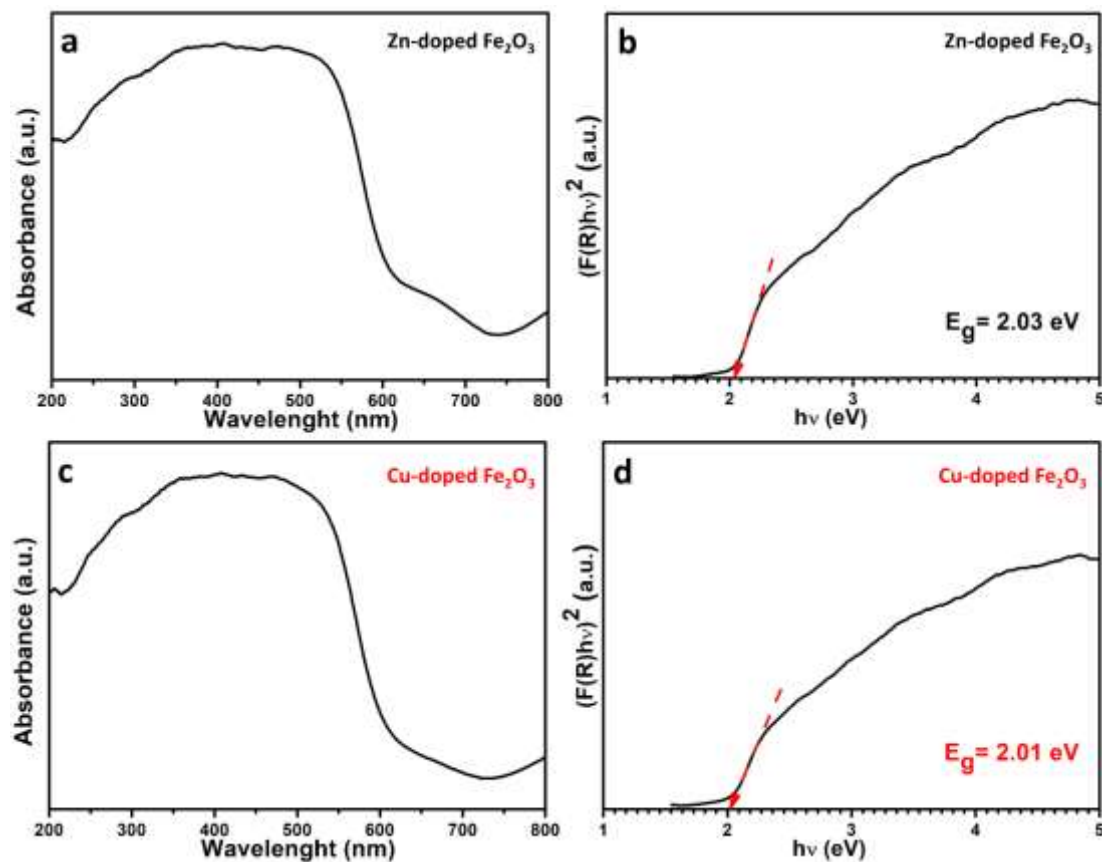


Figure 5. Optical properties and calculated band gap values of the doped-hematite nanoparticles. The absorption spectra of a) Zn-doped hematite and c) Cu-doped hematite and evaluation of bandgaps via Tauc-plots for b) Zn-doped hematite and d) Cu-doped hematite.

Figures 6a and 6b show the changes in the absorption spectra of the rhodamine B aqueous solution exposed to solar simulator over time in the presence of transition metal-doped photocatalysts. The degradation rate of RhB during photocatalytic processes was measured by using Beer-Lambert Law [30]. To determine the degradation rate of the organic dye molecules, the maximum absorbance of the spectrum (given in figure 6a-b) obtained in UV-Vis-NIR spectroscopy was used because peak intensity was directly related to dye concentration in the aqueous solution according to Beer-Lambert Law. The transformed graphics of concentration vs irradiation time belonging to synthesized powders are presented in figure 6c along with other photocatalytic reference results. The spectrum marked as zero minutes indicates adsorption curves at which after adsorption/desorption stability between powder and dye is established by magnetically stirring in the dark for 1 hour. Synthesized transition metal-doped hematite powders almost exhibited identical adsorption properties against dye molecules. In order to be clearly monitored the improvements of the hydrothermally fabricated transition metal-doped hematite photocatalysts against model pollutant dye, photolysis of H_2O_2 and commercial product Degussa TiO_2 nanoparticles, which is a widely used photocatalyst, were also studied. It was observed that there was no degradation in the model pollutant under UV light for 2 hours. The photolysis degradation rate by hydrogen peroxide without photocatalytic nanoparticles was 10,8% after 1 hour under the solar simulator, which is given as a blue line in figure 6c. Degussa TiO_2 powder with an average particle size of 25 nm in size was able to degrade nearly 70% of model pollutant dye in the same duration time. The photocatalytic degradation rate of pollutant molecules executed by Zn-doped hematite nanoparticles, which work in the visible region of the solar spectrum, was slightly higher than the degradation rate performed by the Degussa TiO_2 powder. The Cu-doped hematite nanoparticles exhibited the highest

heterogeneous photocatalytic performance, which was 90% of RhB in an aqueous solution, in the same working time under solar irradiation. This mentioned result is %20 higher than the value obtained by Zn-doped hematite nanoparticles.

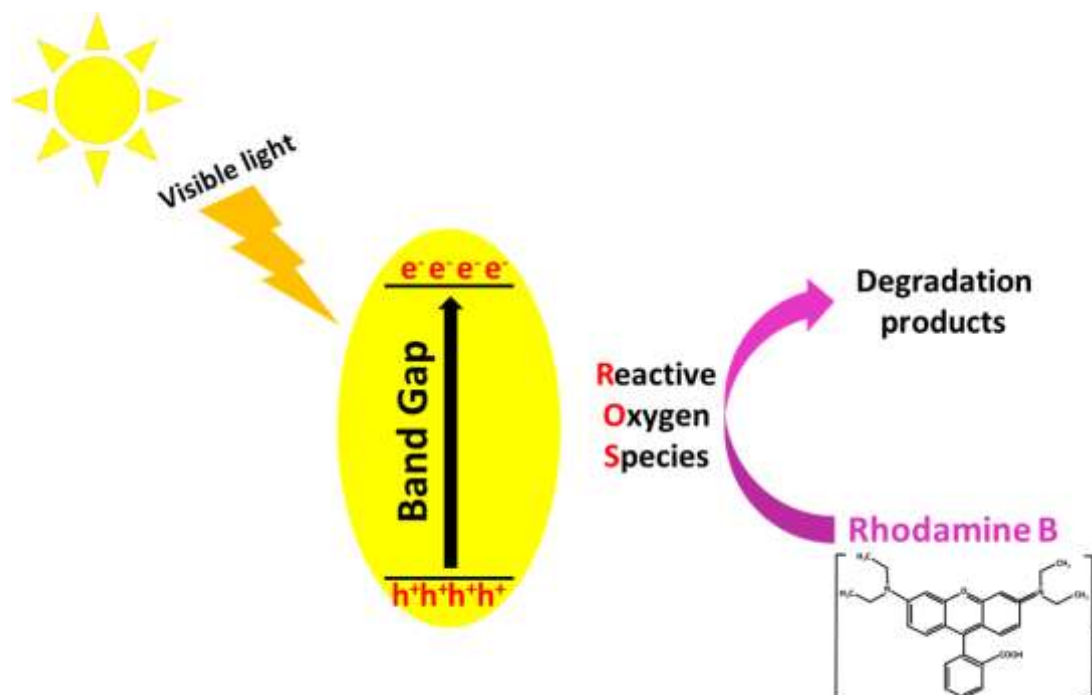


Figure 6. Representative degradation mechanism of the synthesized transition metal doped-hematite photocatalysts against Rhodamine B under solar radiation.

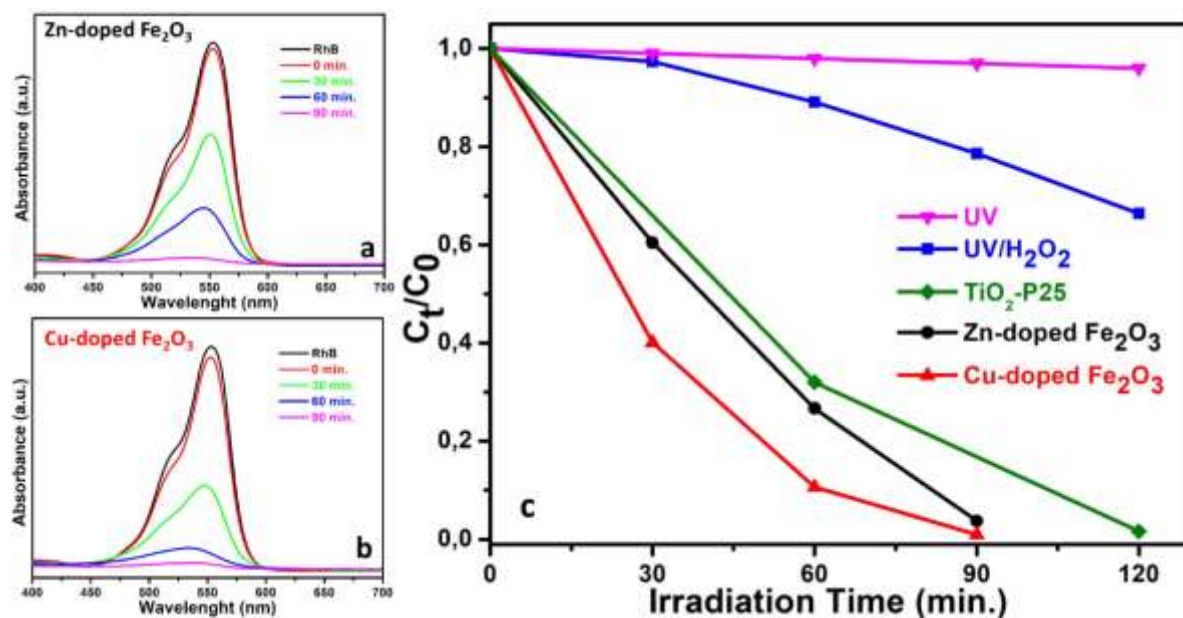


Figure 7. The photocatalytic degradation test results against organic dye of rhodamine B (RhB) under solar simulator. a) absorption spectrum for Zn-doped hematite, b) absorption spectrum for Cu-doped hematite, and c) transformed time-concentration graph related to synthesized doped-hematite photocatalysts along with photolysis results.

The incorporation of Zn²⁺ and/or Cu²⁺ ions in Fe³⁺ sites results in a charge imbalance in the host lattice. one or more of the following mechanisms can take place for compensating charge neutrality: (1) transformation of Fe³⁺ to Fe²⁺ state, (b) filling of oxygen vacancies and (c) formation of cation vacancies.

The substitution effect in hematite at the Fe site influences magnetic, optical, and electrical properties. [31, 32, 33]. Mechanisms providing charge neutrality can lead to improving the life of photo-induced charge carriers, the recombination rate of hole-electron pairs, and electrical conductivity. In the view of photocatalytic applications, the photocatalytic performances of catalysts are boosted such ways mentioned. It is thought that the dopant Cu^{2+} may act as a trap for photogenerated holes and electrons inhibits the recombination of photo-induced charge carriers [34, 23, 35]. Therefore, the lifetime of charge carriers has also been prolonged. As a result of these mechanisms, much more reactive oxygen species (ROS) are generated, and thus, it results in enhanced photocatalytic activity. Moreover, bandgap, which is slightly narrow relative to Zn-doped hematite particles, and more surface defects arising from Cu-dopant might have contributed to the photocatalytic activity of Cu-doped hematite powders.

IV. CONCLUSIONS

Highly photoactive visible-light-driven photocatalyst nanoparticles and nanoparticles included homogeneously distributed dopants were successfully produced by a basic hydrothermal technique. The synthesized transition metal-doped hematite photocatalysts against RhB dye molecule were studied under AM 1.5G solar simulator. It was found that copper was a highly effective dopant and Cu-doped hematite nanoparticles showed better photocatalytic activity (%20 higher) compared with Zn-doped hematite nanoparticles. Furthermore, both synthesized nanoparticles of Zn-doped and Cu-doped hematite exhibited better photocatalytic activity relative to the reference commercial product of Degussa TiO_2 . It was important to note that even though there were no significant differences relative to each other, which strongly influence photocatalytic activity such as morphological features, optical absorption characteristics, and band gaps. The photocatalytic activity of Cu-doped $\alpha\text{-Fe}_2\text{O}_3$ nanoparticles was 20% higher than that of the Zn-doped $\alpha\text{-Fe}_2\text{O}_3$. The synthesized Cu-doped hematite particle is a promising candidate as a visible-light-driven photocatalytic material to degrade pollutants in an aquatic media.

V. REFERENCES

-
- [1] P. Wang, B. Huang, Y. Dai and M.H. Whangbo, "Plasmonic photocatalysts: harvesting visible light with noble metal nanoparticles," *Physical Chemistry Chemical Physics*, vol. 14, no. 28, pp. 9813-9825, 2012.
- [2] K. Sivula, F. Le Formal and M. Grätzel, "Solar water splitting: progress using hematite ($\alpha\text{-Fe}_2\text{O}_3$) photoelectrodes," *ChemSusChem*, vol. 4, no. (4), pp. 432-449, 2011.
- [3] J.H. Kennedy and K.W. Frese, "Flatband Potentials and Donor Densities of Polycrystalline $\alpha\text{-Fe}_2\text{O}_3$ Determined from Mott-Schottky Plots," *Journal of the Electrochemical Society*, vol. 125, no. 5, pp. 723-726, 1978.
- [4] A.J. Bosman and H.J. Van Daal, "Small-polaron versus band conduction in some transition-metal oxides," *Advances in Physics*, vol. 19, no. 77, pp. 1-117, 1970.
- [5] K. Itoh and J.M. Bockris, "Thin film photoelectrochemistry: iron oxide," *Journal of the Electrochemical Society*, vol. 131, no. 6, pp. 1266-1271, 1984.
- [6] N.J. Cherepy, , D.B. Liston, J.A. Lovejoy, H. Deng and J.Z. Zhang, " Ultrafast studies of photoexcited electron dynamics in γ - and $\alpha\text{-Fe}_2\text{O}_3$ semiconductor nanoparticles," *The Journal of Physical Chemistry B*, vol. 102, no. 5, pp. 770-776, 1998.

-
- [7] S.C. Warren, K. Voitchovsky, H. Dotan, C.M. Leroy, M. Cornuz, F. Stellacci, C. Hébert, A. Rothschild and M. Grätzel, "Identifying champion nanostructures for solar water-splitting," *Nature materials*, vol. 12, no. 9, pp.842-849, 2013.
- [8] M. Li, Y. Yang, Y. Ling, W. Qiu, F. Wang, T. Liu, Y. Song, X. Liu, P. Fang, Y. Tong and Y. Li, "Morphology and doping engineering of Sn-doped hematite nanowire photoanodes," *Nano letters*, vol. 17, no. 4, pp. 2490-2495, 2017.
- [9] L. Xi, P.S. Bassi, S.Y. Chiam, W.F. Mak, P.D. Tran, J. Barber, J.S.C. Loo and L.H. Wong, "Surface treatment of hematite photoanodes with zinc acetate for water oxidation," *Nanoscale*, vol. 4, no. 15, pp. 4430-4433, 2012.
- [10] E. Alp, R. İmamoğlu, U. Savacı, S. Turan, M.K. Kazmanlı and A. Genç, "Plasmon-enhanced photocatalytic and antibacterial activity of gold nanoparticles-decorated hematite nanostructures," *Journal of Alloys and Compounds*, vol. 852, pp.157021, 2021.
- [11] V. Kumar, D.S. Ahlawat, S.A. Islam and A. Singh, "Ce doping induced modifications in structural, electrical and magnetic behaviour of hematite nanoparticles," *Materials Science and Engineering: B*, vol. 272, pp.115327, 2021.
- [12] J. Cai, H. Liu, C. Liu, Q. Xie, L. Xu, H. Li, J. Wang and S. Li, "Enhanced photoelectrochemical water oxidation in hematite: accelerated charge separation with co doping," *Applied Surface Science*, vol. 568, pp. 150606, 2021.
- [13] Y. Ling, G. Wang, D.A. Wheeler, J.Z. Zhang and Y. Li, "Sn-doped hematite nanostructures for photoelectrochemical water splitting," *Nano letters*, vol. 11, no. 5, pp.2119-2125, 2011.
- [14] S.M. Tao, L.Y. Lin and D. Zhou, "Developing hematite homojunction with titanium and magnesium dopants for photocatalyzing water oxidation," *International Journal of Hydrogen Energy*, vol. 46, no. 9, pp. 6321-6328, 2021.
- [15] J. Huang, G. Hu, Y. Ding, M. Pang and B. Ma, "Mn-doping and NiFe layered double hydroxide coating: effective approaches to enhancing the performance of α -Fe₂O₃ in photoelectrochemical water oxidation," *Journal of Catalysis*, vol. 340, pp. 261-269, 2016.
- [16] A. Kay, D.A. Grave, D.S. Ellis, H. Dotan and A. Rothschild, "Heterogeneous doping to improve the performance of thin-film hematite photoanodes for solar water splitting," *ACS Energy Letters*, vol. 1, no. 4, pp. 827-833, 2016.
- [17] M. Mohapatra, S. Layek, S. Anand, H.C. Verma and B.K. Mishra, "Structural and magnetic properties of Mg-doped nano- α -Fe₂O₃ particles synthesized by surfactant mediation-precipitation technique," *physica status solidi (b)*, vol. 250, no. 1, pp. 65-72, 2013.
- [18] H.W. Chang, Y. Fu, W.Y. Lee, Y.R. Lu, Y.C. Huang, J.L. Chen, C.L. Chen, W.C. Chou, J.M. Chen, J.F. Lee and S. Shen, "Visible light-induced electronic structure modulation of Nb- and Ta-doped α -Fe₂O₃ nanorods for effective photoelectrochemical water splitting," *Nanotechnology*, vol. 29, no. 6, pp. 064002, 2018.
- [19] A. Ahmadi-Arpanah, H. Meleki-Ghaleh, Z. Dargahi, P. Khademi-Azandehi, G. Mirzaei, Y. Beygi-Khosrowshahi and M.H. Siadati, "The photocatalytic antibacterial behavior of Cu-doped nanocrystalline hematite prepared by mechanical alloying," *Applied Nanoscience*, vol. 11, no. 3, pp. 817-832, 2021.
- [20] X. Zhang, H. Li, S. Wang, F.R.F. Fan and A.J. Bard, "Improvement of hematite as photocatalyst by doping with tantalum," *The Journal of Physical Chemistry C*, vol. 118, no. 30, pp. 16842-16850, 2014.

-
- [21] L. Wang, C.Y. Lee and P. Schmuki, "Ti and Sn co-doped anodic α -Fe₂O₃ films for efficient water splitting," *Electrochemistry communications*, vol. 30, pp. 21-25, 2013.
- [22] D. Cao, W. Luo, M. Li, J. Feng, Z. Li and Z. Zou, "A transparent Ti⁴⁺ doped hematite photoanode protectively grown by a facile hydrothermal method" *CrystEngComm*, vol. 15, no. 13, pp. 2386-2391, 2013.
- [23] R. Satheesh, K. Vignesh, A. Suganthi and M. Rajarajan, "Visible light responsive photocatalytic applications of transition metal (M= Cu, Ni and Co) doped α -Fe₂O₃ nanoparticles," *Journal of environmental chemical engineering*, vol. 2, no. 4, pp. 1956-1968, 2014.
- [24] P. Kubelka, "New contributions to the optics of intensely light-scattering materials. Part I," *Journal of the Optical Society of America*, vol. 38, no. 5, pp. 448-457, 1948.
- [25] J. Tauc, Optical properties of amorphous semiconductors, *Amorphous and Liquid Semiconductors*, 1st ed., Boston, USA: Springer, 1974, ch. 4, pp. 159-220.
- [26] S. Piccinin, "The band structure and optical absorption of hematite (α -Fe₂O₃): a first-principles GW-BSE study," *Phys. Chem. Chem. Phys.*, vol. 21, no. 6, pp. 2957-2967, 2019.
- [27] W. H. Glaze, J. W. Kang and D. H. Chapin, "The chemistry of water treatment processes involving ozone, hydrogen peroxide and ultraviolet radiation," *Ozone Sci. Eng.*, vol. 9, no. 4, pp. 335-352, 1987.
- [28] J.M. Poyatos, M.M. Muño, M.C. Almecija, J.C. Torres, E. Hontoria and F. Osorio, "Advanced oxidation processes for wastewater treatment: state of the art," *Water, Air, and Soil Pollution*, vol. 205, no. 1-4, pp. 187, 2010.
- [29] M.A. Rauf and S.S. Ashraf, "Fundamental principles and application of heterogeneous photocatalytic degradation of dyes in solution," *Chemical engineering journal*, vol. 151, no. 1-3, pp. 10-18, 2009.
- [30] D.F. Swinehart, "The beer-lambert Law," *J. Chem. Educ.*, vol. 39, no. 7, pp. 333, 1962.
- [31] A. Lassoued, M.S. Lassoued, B. Dkhil, A. Gadri and S. Ammar, "Structural, optical and morphological characterization of Cu-doped α -Fe₂O₃ nanoparticles synthesized through co-precipitation technique," *Journal of Molecular Structure*, vol. 1148, pp. 276-281, 2017.
- [32] S. Chahal, A. Kumar and P. Kumar, "Zn doped α -Fe₂O₃: an efficient material for UV driven photocatalysis and electrical conductivity," *Crystals*, vol. 10, no. 4, pp. 273, 2020.
- [33] A. Yogi and D. Varshney, "Magnetic and structural properties of pure and Cr-doped haematite: α -Fe_{2-x}Cr_xO₃ (0 ≤ x ≤ 1)," *Journal of Advanced Ceramics*, vol. 2, no. 4, pp.360-369, 2013.
- [34] Z.D. Pozun and G. Henkelman, "Hybrid density functional theory band structure engineering in hematite," *The Journal of chemical physics*, vol. 134, no. 22, pp. 224706, 2011.
- [35] X.Y. Meng, G.W. Qin, S. Li, X.H. Wen, Y.P. Ren, W.L. Pei and L. Zuo, "Enhanced photoelectrochemical activity for Cu and Ti doped hematite: The first principles calculations," *Applied Physics Letters*, vol. 98, no. 11, pp.112104, 2011.